THE ASTROPHYSICAL JOURNAL, 494:535–545, 1998 February 20

DECOUPLED AND INHOMOGENEOUS GAS FLOWS IN S0 GALAXIES

A. D'ERCOLE AND L. CIOTTI
Osservatorio Astronomico di Bologna, via Zamboni 33, 40126 Bologna, Italy
Received 1997 June 9; accepted 1997 September 30

ABSTRACT

A recent analysis of the *Einstein* sample of early-type galaxies has revealed that at any fixed optical luminosity L_B, S0 galaxies have lower mean X-ray luminosity L_X per unit L_B than elliptical galaxies. Following a previous analytical investigation of this problem (Ciotti & Pellegrini), we have performed two-dimensional numerical simulations of the gas flows inside S0 galaxies in order to ascertain the effectiveness of rotation and/or galaxy flattening in reducing the L_X/L_B ratio.

The flow in models without supernova (SNIa) heating is considerably ordered, and essentially all the gas lost by the stars is cooled and accumulated in the galaxy center. If rotation is present, the cold material settles in a disk on the galactic equatorial plane. Models with a time-decreasing SNIa heating host gas flows that can be much more complex. After an initial wind phase, gas flows in energetically strongly bound galaxies tend to reverse to inflows. This occurs in the polar regions, while the disk is still in the outflow phase. In this phase of strong decoupling, cold filaments are created at the interface between inflowing and outflowing gas. Models with more realistic values of the dynamical quantities are preferentially found in the wind phase with respect to their spherical counterparts of equal L_B. The resulting L_X of this class of models is lower than in spherical models with the same L_B and SNIa heating. At variance with cooling flow models, rotation is shown to have only a marginal effect in this reduction, while the flattening is one of the driving parameters for such underluminosity, in accordance with the analytical investigation.

Subject headings: galaxies: cooling flows — galaxies: elliptical and lenticular, cD — galaxies: kinematics dynamics — galaxies: structure — methods: numerical — X-rays: galaxies

1. INTRODUCTION

It is well known that normal early-type galaxies are X-ray emitters, with 0.2–4 keV luminosities ranging from $\sim 10^{40}$ to $\sim 10^{43}$ ergs s^{-1}. The X-ray luminosity L_X is found to correlate with the blue luminosity L_B ($L_X \propto L_B^{2.0\pm0.2}$), but there is a large scatter of roughly 2 orders of magnitude in L_X at any fixed $L_B > 3 \times 10^{10}\ L_\odot$ (Fabbiano 1989; Fabbiano, Kim, & Trinchieri 1992).

The trend and the scatter in the $L_X - L_B$ diagram have been successfully reproduced by the time-dependent, one-dimensional hydrodynamic models of Ciotti et al. (1991, hereafter CDPR). In these models, the gas lost by the evolving stars is heated to X-ray temperatures by stellar random motions and supernova (SNIa) explosions. Given the assumed time dependence of both mass loss rate ($\propto t^{-1.36}$) and SNIa rate ($\propto t^{-1.5}$), the CDPR models can evolve through up to three different dynamical phases, i.e., from winds to subsonic outflows to inflows (in the following, we call this kind of evolution the WOI sequence). CDPR introduced the *global* parameter χ in order to predict the dynamical status of the gas flows in nonrotating, spherical galaxies. This parameter was defined as the ratio between the power required to extract steadily the gas supplied by the mass loss of the evolving stellar population from the galaxy potential well, L_g, and the power supplied to the gas by the thermalization of the stellar random motions and by the supernova heating (L_σ and $L_{\rm SN}$, respectively). Because of the temporal evolution of the various source terms, χ is an increasing function of time. Numerical simulations showed the correspondence between $\chi < 1$ and the presence of a wind phase (i.e., of a low L_X), and the onset of a high L_X soon after χ becomes greater than 1.

A recent analysis of the complete *Einstein* sample of early-type galaxies showed that on average S0 galaxies have lower L_X and L_X/L_B than elliptical galaxies (Es) (Eskridge, Fabbiano, & Kim 1995a, 1995b). A possible explanation of this fact could be that S0s and nonspherical Es are less able to retain hot gaseous haloes than rounder systems of the same L_B. This could be due to a lower gravitational energy, because of their higher rotation rate, which decreases the effective potential, or their different mass distribution. A theoretical analysis of this problem—based on the global energetics of the X-ray–emitting gas—was carried out by Ciotti & Pellegrini (1996, hereafter CP). They generalized the global parameter χ for flows in flat and rotating two-component galaxy models. In particular, they added to χ the contribution of the ordered rotation of the galaxy stellar component, $L_{\rm rot}$, showing that, at least from a global point of view, rotation alone cannot change an energetically bound gas flow to an unbound one (see § 2.3). On the contrary, using two-component Miyamoto & Nagai (1975, hereafter MN) models, and under the assumption of an identical rate of SNIa per unit L_B in S0s and Es, CP showed that flat galaxies can have a much lower χ than rounder ones of the same luminosity, due essentially to their flattening, even in the presence of massive spherical dark haloes. More precisely, they showed how a realistic flattening can produce a decrease of L_g of $\sim 20\%$, a result that can be sufficient to change an inflow into a wind. So, the effect of the flattening was suggested as a possible explanation for the S0 underluminosity. Incidentally, note that the decrease in the gravitational energy that is released by a stationary inflow at the bottom of the galactic potential well, associated to the decrease of L_g, does not lower signifi-

cantly the L_X of pure cooling flow models (see Fig. 1 in CDPR).

Despite the possible agreement between the observations and the results of CP, this purely energetical approach can be seriously questioned considering the complexity of two-dimensional gas flows and the fact that χ is a global quantity. In fact *decoupled flows*—in which at the same time different parts of the galaxy are in inflow and outflow—may in principle develop in the CDPR scenario in such a way that L_X remains high even if $\chi < 1$; if this is the case, $\chi < 1$ cannot be used as a reliable indicator for a low X-ray luminosity, and the analysis of CP is seriously questioned.

Two-dimensional numerical simulations of gas flows in early-type galaxies were actually carried out by Kley & Mathews (1995, hereafter KM) and Brighenti & Mathews (1996, hereafter BM). These simulations, however, considered only pure cooling flows for which the flow decoupling is not expected. KM considered rotating spherical King models plus a spherical quasi-isothermal dark halo, without SNIa heating. Successively BM considered oblate galaxies with different axial ratios, sustained by various amounts of ordered and disordered kinetic energies. They assumed an SNIa rate $\propto t^{-1}$, with a present day value of one-tenth of that proposed by Tammann (1982). Their models show that the gas flow and the associated L_X are only slightly dependent on the flattening of the galaxy (in agreement with the CP analysis applied to the *inflow* case) and that L_X is reduced by increasing the amount of ordered rotation. These two-dimensional hydrodynamical models do not solve problems such as the disposal of excessive amounts of cold gas (a problem already encountered in one-dimensional pure cooling flow models) on an equatorial disk, which is actually unobserved, and the excessively flat shape of the X-ray isophotes when compared with the observations.

Motivated by the given arguments, we adopt the same input physics used for the hydrodynamical equations in CDPR, in order to explore whether the WOI sequence is still achieved in flat galaxies, how such a sequence is influenced by galaxy flattening and rotation, how important the decoupling in the flow is, which observational consequences are predicted in this case, and finally whether the energetical

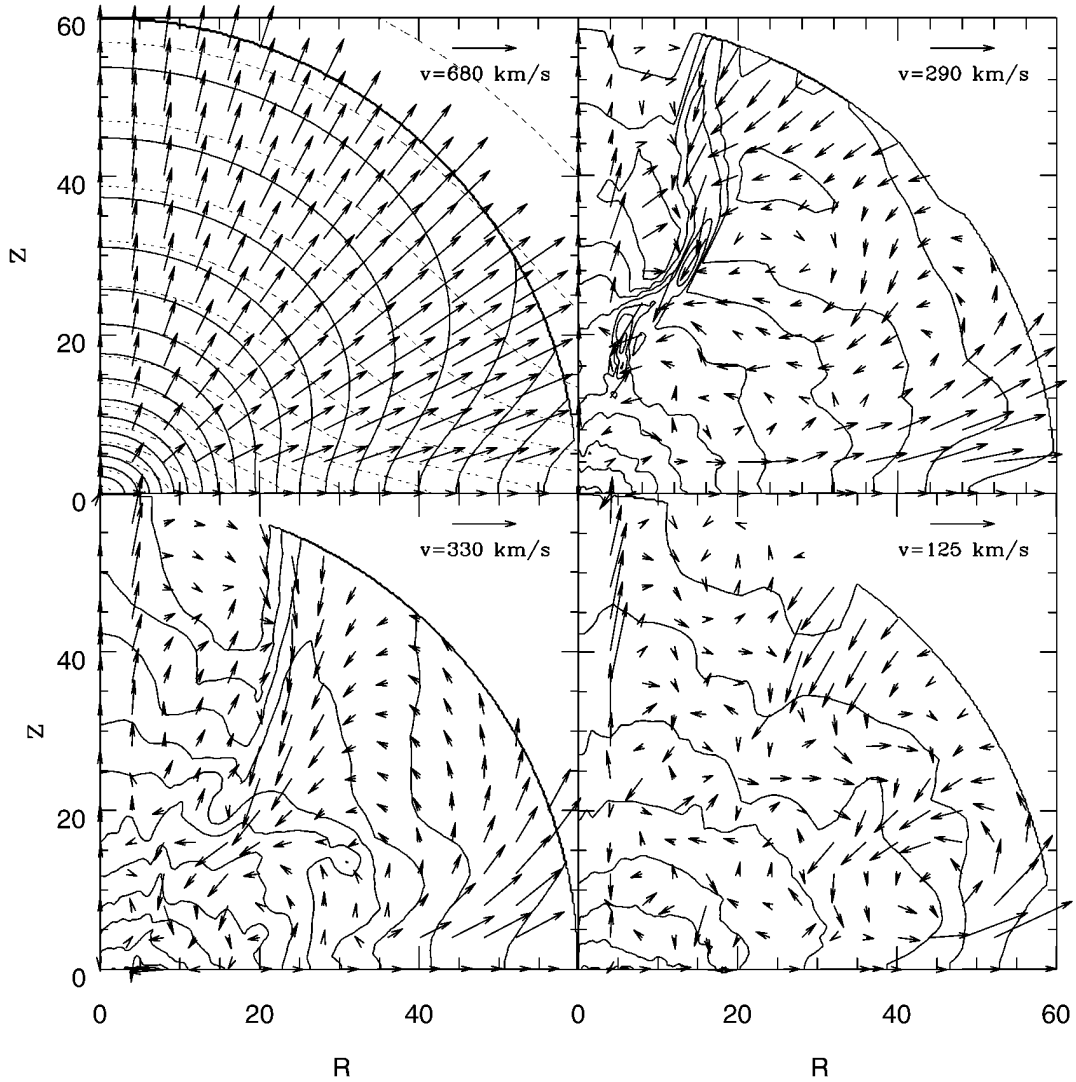

FIG. 1.—Gas density and velocity fields of model A1 at four different times (0.46, 2.16, 3.37, and 15) Gyr (*top left, top right, bottom left, and bottom right*). In the top left panel the dashed lines represent the stellar density distribution. In the top right panel the large high-density transient structure is apparent. Note how the velocity field in the top right and bottom left panels is dominated by large vortices, while in the bottom right panel the velocity is very low, and nearly random. Labels are in kiloparsecs.

explanation of CP is exhaustive. This is accomplished with two different classes of models. In the first we compare the behavior of the gas flow in spherical and flat galaxies that are *energetically globally equivalent* (both with and without SNIa heating). In the second class of simulations we investigate the gas flows in realistic galaxy models of S0s, also in order to explore the possibility of flow decoupling in galaxies with $\chi < 1$ and its effects on L_X.

We thus study the evolution of gas flows in the galaxy models constructed and described in detail by CP, i.e., axisymmetric stellar and dark mass distributions with the MN shape, and in which the internal dynamics is determined by the solution of the associated Jeans equations, allowing for variable amounts of ordered rotation and velocity dispersion.

In § 2 we briefly describe the models used in the simulations. In § 3 the results obtained for models with different amounts of ordered rotation, SN heating, flattening, and characteristic scale length are presented. A discussion, considering also some recent observational results, is given in § 4, and in § 5 the main conclusions are summarized.

2. THE MODELS

2.1. *The Galaxy Density Distribution*

The two-component mass models used in our simulations and their internal dynamics are fully discussed in CP, which includes the explicit analytical formulae for the various terms in the virial theorem and for χ. Here only the basic formulae are reported. The stellar density distribution is given by

$$\rho_* = \left(\frac{M_* b^2}{4\pi}\right) \frac{aR^2 + (a + 3\zeta)(a + \zeta)^2}{\zeta^3[R^2 + (a + \zeta)^2]^{5/2}}, \quad (1)$$

and its potential is

$$\Phi_* = -\frac{GM_*}{\sqrt{R^2 + (a + \zeta)^2}}, \quad (2)$$

where $\zeta = (z^2 + b^2)^{1/2}$ and (R, φ, z) are the cylindrical coordinates (MN).[1] The dark matter halo is described by another MN density distribution characterized by M_h, a_h, and b_h. The associated Jeans equations are solved in the total potential $\Phi_{\rm tot} = \Phi_* + \Phi_h$, and under the assumption that the distribution function depends only on the specific energy and the angular momentum component along the z-axis (see, e.g., Binney & Tremaine 1987, p. 197). With this assumption, the radial and axial velocity dispersions are equal, i.e., $\sigma_{\rm R} = \sigma_z \equiv \sigma$, and the only nonzero streaming motion can be in the azimuthal direction (φ). The intrinsic degeneracy in the azimuthal velocity component is removed adopting the Satoh (1980) k-decomposition, i.e.,

$$\overline{v_\varphi}^2 = k^2(\overline{v_\varphi^2} - \sigma^2), \quad (3)$$

$$\sigma_\varphi^2 \equiv \overline{v_\varphi^2} - \overline{v_\varphi}^2 = k^2\sigma^2 + (1 - k^2)\overline{v_\varphi^2}, \quad (4)$$

with $0 \le k \le 1$, where $\overline{v_\varphi}$ is the modulus of the ordered rotational velocity of the galactic stellar component. In the case $k = 0$, no net rotation is present and all the flattening is due to σ_φ^2; $k = 1$ corresponds to the isotropic rotator. The analytical solutions of the Jeans equations can be obtained for $b_h = b$. In the case of $a_h = a$, the formulae for the velocity components are expressed in terms of elementary functions and are given in CP together with their edge-on projection.

[1] When $a = 0$, the density distribution (1) reduces to the Plummer (1911) model, and b becomes its effective radius. So, b can be roughly considered a characteristic scale length, while the galaxy flattening is determined by the dimensionless ratio $s = a/b$.

2.2. *The Hydrodynamical Equations*

The equations describing the gas flows in our simulations are

$$\frac{\partial \rho}{\partial t} + \nabla \cdot (\rho \boldsymbol{v}) = \alpha \rho_*, \quad (5)$$

$$\frac{\partial \boldsymbol{m}}{\partial t} + \nabla \cdot (\boldsymbol{m} \otimes \boldsymbol{v}) = -(\gamma - 1)\nabla E + \boldsymbol{g}\rho + \alpha \rho_* \boldsymbol{v}_*, \quad (6)$$

$$\frac{\partial E}{\partial t} + \nabla \cdot (E\boldsymbol{v}) = -(\gamma - 1)E\nabla \cdot \boldsymbol{v} - L + \alpha \rho_* \left(\epsilon_0 + \frac{1}{2} \| \boldsymbol{v} - \boldsymbol{v}_* \|^2\right), \quad (7)$$

where $\boldsymbol{v}$ is the fluid velocity, and ρ, $\boldsymbol{m}$, and E are the mass, the momentum, and the internal energy of the gas per unit volume, respectively. The source terms on the right-hand sides of equations (5)–(7) describe the injection of mass, momentum and energy in the gas due to the mass return and energy input from the stars. $\alpha(t) = \alpha_*(t) + \alpha_{\rm SN}(t)$ is the specific mass return rate from stars and SNIa, respectively, with $\alpha_* \propto t^{-1.36}$ and $\alpha_{\rm SN} \propto t^{-1.5}$; ϵ_0 is the injection energy per unit mass due to the stellar random motions and to SNIa explosions. $\boldsymbol{v}_*$ is the bulk velocity of the stars, whose modulus is given by equation (3), $\boldsymbol{g} = -\nabla\Phi_{\rm tot}$ is the gravitational acceleration due to the total mass distribution, and $\gamma = 5/3$. Finally, $L = n_{\rm e} n_{\rm p} \Lambda(T)$ is the cooling rate per unit volume, where for the cooling law $\Lambda(T)$ we follow the prescription of Mathews & Bregman (1978). For more details on the exact form of $\alpha_*(t)$, $\alpha_{\rm SN}(t)$ and ϵ_0, see CDPR and KM.

To integrate the set of equations we used a second-order, upwind, two-dimensional extension of the numerical code described in CDPR, coupled with a staggered, spherical, Eulerian grid. Given the symmetry of the problem, the grid covers polar angles $0° \le \theta \le 90°$ with 40 equally spaced angular zones, and reflecting boundary conditions are applied at $\theta = 0°$ and $\theta = 90°$. The radial coordinate covers the range $0 \le r = (R^2 + z^2)^{1/2} \le 100$ kpc with 80 logarithmically spaced zones, and a free outflow from the grid is allowed at the outer edge. At the inner edge reflecting boundary conditions are set. We assume the model galaxies to be initially devoid of gas due to the previous activity of the Type II SNs. A discussion on the reliability and implications of this assumption is given in CDPR.

2.3. *The χ-Parameter*

The main ingredients of the global parameter χ are presented here. The SNIa heating evolution is parameterized as $L_{\rm SN} = 10^{51} R_{\rm SN} L_B$ ergs s^{-1}, with

$$R_{\rm SN} = 0.88\ h^2\ {\rm SNU}\ \vartheta_{\rm SN} \left(\frac{t}{15\ {\rm Gyr}}\right)^{-1.5}, \quad (8)$$

where $h = H_0/100$ km s^{-1} Mpc^{-1}, and 1 SNU = 1 SN per century per 10^{10} $L_\odot$ (see CDPR). When $t = 15$ Gyr, $L_B = 10^{10}$ $L_\odot$ and $\vartheta_{SN} = 1$, the standard SNIa rate is recovered (Tammann 1982).[2]

The power L_g required to extract steadily from the galaxy the mass losses from the aging stellar population is

$$L_g = \alpha(t) \int \rho_* |\Phi_{tot}| \, dV \, . \quad (9)$$

The thermalization of the stellar random motions heats the gas at a power L_σ given by

$$L_\sigma = \frac{\alpha(t)}{2} \int \rho_* (2\sigma^2 + \sigma_\varphi^2) \, dV \, , \quad (10)$$

while the power L_{rot} related to the ordered fraction of the kinetic energy is given by

$$L_{rot} = \frac{\alpha(t)}{2} \int \rho_* \overline{v_\varphi}^2 \, dV \, . \quad (11)$$

Unfortunately this last term cannot be inserted in the χ definition in a simple way. In fact, two opposite and extreme scenarios can be assumed: one in which also L_{rot} is thermalized (contributing to the gas heating together with L_σ and L_{SN}), and another in which the only effect of L_{rot} is to reduce the depth of the effective galactic potential well. As a consequence, the global parameter χ is defined as

$$\chi = \frac{L_g - \gamma L_{rot}}{L_{SN} + L_\sigma + (1 - \gamma) L_{rot}} \, , \quad (12)$$

with $0 \le \gamma \le 1$. Note that if $\gamma = 0$, i.e., in the case of *complete thermalization*, the virial theorem implies that $L_\sigma + L_{rot}$ depends only on the galaxy structure and χ is independent of the amount of ordered rotation (in our case, of the value of the parameter k). When instead $\gamma = 1$, i.e., in the case of *cold rotation*, the effect of rotation is maximum; CP showed that also in this case, for realistic galaxy models the differences in the value of χ, for a null and a maximum ordered velocity configuration, are small, usually less than 10%. Moreover whenever $\gamma > 0$ the introduction of rotation decreases a $\chi < 1$ and increases a $\chi > 1$. In conclusion, from the CP analysis it results that rotation alone cannot invert the global energy balance of a gas flow, but can help the occurrence of the wind when $\chi < 1$. Due to the small dependence of χ on γ, through the paper we assume $\gamma = 0$.

3. THE RESULTS

3.1. *Model A1:* $\vartheta_{SN} = 0.3$ *and* $k = 1$

We describe here in detail the main characteristics of the flow hosted by a galaxy model in which ordered rotation ($k = 1$) and SNIa heating in accordance with the latest estimates of Cappellaro et al. (1997, $\vartheta_{SN} = 0.3$) are present. We assume $M_* = 2.75 \times 10^{11}$ $M_\odot$, $M_*/L_B = 5.5$, so that $L_B = 5 \times 10^{10}$ $L_\odot$, and $a = b = 3$ kpc. The dark halo has the same profile of the stellar distribution, i.e., $a_h = a$ and $b_h = b$, and $M_h/M_* = 2$ (see Table 1). The three-dimensional central velocity dispersion is $\sigma_c = 330$ km s^{-1}, and the maximum of the ordered rotational velocity is $v_{rot} = 360$ km s^{-1}. This set of parameters is such that $\chi = 1$ at the present epoch, in order to compare as much as possible the present results with those obtained for the so-called *reference model* discussed in CDPR (hereafter KRM, $\chi_{KRM} = 1.1$). L_B is also the same of the KRM, so that the mass return rate of the two models is exactly the same. Note how it turns out that, in order to keep $\chi = 1$, model A1 must have very high stellar σ_c and v_{rot}. This is not a surprise: in fact, as already pointed out by CP, in a realistic flat model with a nonnegligible ϑ_{SN}, the present-epoch χ is substantially lower than unity. The same comment applies to models A1–A4.

TABLE 1

MODELS PARAMETERS

Model[a]	b[b]	a/b	σ_c[c]	v_{rot}[d]	ϑ_{SN}	k	χ[e]	t_{cc}[f]	t_{fil}[f]
A1	3	1	330	360	0.3	1	1	2	2
A2	3	1	330	0	0.3	0	1	1.7	1.7
A3	3	0.7	376	365	0.3	1	1.20	1.4	1.4
A4	3	1.3	300	347	0.3	1	0.94	3	3
B1	3	1	330	360	0.0	1	4	0	...
B2	3	1	330	0	0.0	0	4	0	...
C1	4	1	290	309	0.3	1	0.85	5.5	10.5
C2	4	1.3	260	300	0.3	1	0.75	...	...
D1	5	1	258	277	0.3	1	0.70	...	...
D2	5	0.6	305	283	0.3	1	0.86	5.5	...

[a] All models have $L_B = 10^{10} L_\odot$, $M_* = 10^{11}$ $M_\odot$, and $M_h/M_* = 2$.
[b] In kpc.
[c] Three-dimensional central velocity dispersion in km s^{-1}.
[d] Maximum rotational velocity in km s^{-1}.
[e] For the rotating models computed under the assumption of complete thermalization of ordered motions.
[f] In Gyr.

3.1.1. *Hydrodynamics*

As a consequence of the early high SNIa energy injection, due to the assumed ϑ_{SN} value and $\alpha_{SN} \propto t^{-1.5}$, at the very beginning the flow is in the wind supersonic phase, i.e., the radial velocity $v_r(R, z) > v_{sound}(R, z)$ throughout the galaxy (Fig. 1, *top left panel*).

As time increases and the energetic input decreases according to equation (8), the sonic surface moves outward, with u_r decreasing earlier in the central regions of the galaxy, and the gas density increases. Finally, because of the rapidly increasing radiative losses (the so-called cooling catastrophe), at $t_{cc} \simeq 2$ Gyr the fluid starts to revert its motion in a conical region containing the polar axis. We call this phenomenon *flow inversion* and the subsequent flow *decoupled inflow*. The most striking feature of this evolutionary phase is the formation of cold, dense *filaments* at the boundary where two streams of inflowing and outflowing gas converge, as can be seen in Figure 1 (*top right panel*). This filamentary phase, which in model A1 suddenly develops at $t_{fil} \simeq t_{cc}$, is rather short ($\lesssim 2$ Gyr). Later on, no more filaments are generated, and the previous ones are accreted at the galactic center. However, regions of gas colder than X-ray temperature and with a low-density contrast are present for a much longer time. During this evolutionary phase two qualitatively different regimes are present: an inner zone ($r \lesssim 15$ kpc), in which the fluid is rather turbulent, and an outer zone, where the velocity field is smooth (Fig. 1, *bottom left panel*). The inflow region becomes progressively larger and larger. At $t = 15$ Gyr the gas is still outflowing in the outskirts of the disk. The flow in the rest of the galaxy is in a turbulent state, characterized by very subsonic velocities ($\| \boldsymbol{v} \| < 5 \times 10^6$ cm s^{-1}, Fig. 1, *bottom right panel*).

[2] Note that in our models the assumed L_B is independent of h. As a consequence, L_{SN} *depends* on h. In the paper we adopt $h = \frac{1}{2}$.

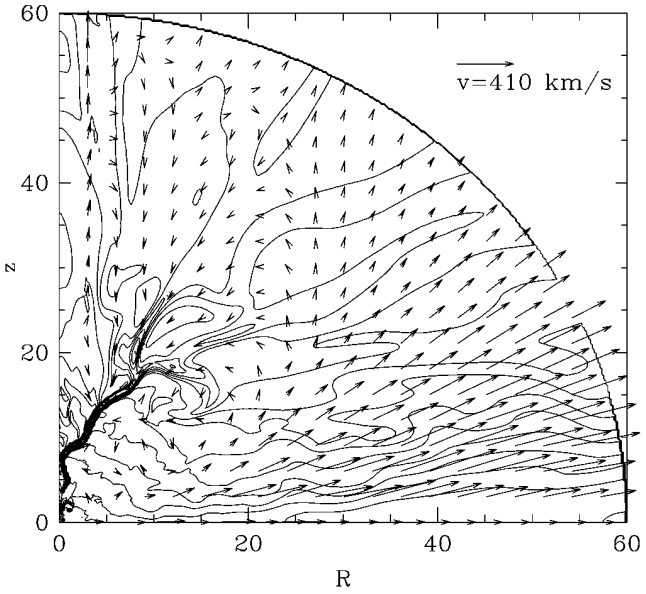

FIG. 2.—Gas temperature and velocity for model A1 (high-resolution simulation) at $t \simeq 2$ Gyr, when the cold filament is completely developed. Note how the disk is still strongly degassing.

In order to understand better the structure of the cold filaments, we performed a high-resolution simulation (with 300 radial meshes and 140 angular meshes covering the same physical space as the normal resolution simulations). Because of the severe limitation due to the azimuthal time step, we could not extend the simulation over 15 Gyr. We thus remapped onto the finer grid the hydrodynamical variables computed on the coarse grid at a time immediately before the filament formation, and we carried on the simulation for the entire lifetime of the filament. Figure 2 shows the temperature and velocity field at $t = 2$ Gyr. Density and temperature vary along the filament. For $r \lesssim 20$ kpc, $\rho_{\rm fil} \sim 6.3 \times 10^{-27}$ g cm^{-3}, and the density contrast between the cold filaments and the surrounding density is on the order of 30. The mean temperature is $T_{\rm fil} \simeq 10^4$ K (the lowest allowed temperature in our simulations). At large r the density decreases and the temperature increases, but never reaches X-ray temperatures. We did not made convergence tests, so it is plausible that the filaments are denser and thinner. We stress that in our two-dimensional simulations, these filaments are in fact surfaces. This fact should be kept in mind in all the following discussions.[3]

The cold gas accreted during the entire lifetime of the galaxy forms a small disk, whose radius oscillates around a mean value of 3 kpc. The total mass of the cold disk is $1.5 \times 10^{10}\ M_\odot$, while the hot X-ray gas is $6.3 \times 10^8\ M_\odot$ (Fig. 3*b*, *dotted line 1*), much less than the hot gas in the equivalent KRM in CDPR ($\sim 5.4 \times 10^9\ M_\odot$).

3.1.2. *Energetics*

The comparison with the KRM is instructive. Also for this spherically symmetric model the present day $\chi \simeq 1$, but $t_{\rm cc} \simeq 10$ Gyr, much later than in model A1. From Figure 3*d* we note that the time evolution of L_X (*dotted line 1*) is qualitatively similar to that of spherical models. After an initial decrease during the wind phase, L_X increases up to a maximum value at $t = 2.5$ Gyr. Later on, L_X decreases again, in pace with the decreasing mass return from the stars. When L_X reaches its maximum, a nonnegligible fraction of gas is still outflowing from the galaxy, as in the one-dimensional models. Note that at the flow inversion the energy budget ($\chi < 1$) indicates that the SNIa energy injection would be able to sustain a global outflow. This means that, because of the strong decoupling of the flow, in this model the global energetic argument (i.e., the χ value), is not a useful indicator of the dynamical state of the gas.

A second important difference between spherical models and model A1 must be stressed: in the latter, L_X is a factor of 4 fainter than $L_{\rm SN}$ (Fig. 3*d*, *solid line*), at variance with one-dimensional models in which L_X may be even greater than $L_{\rm SN}$ in the inflow phase. The fainter L_X of model A1 is due to its lower content of hot gas with respect to the KRM (see § 3.1.1). This lower fraction of hot gas is due to the higher efficiency of the cooling near the equatorial plane of model A1, a natural consequence of a higher gas density in this region, which in turn is due to the higher local stellar density (the effect of rotation will be discussed in § 3.1.4)

We note however that, although the hot gas mass in model A1 is lower by about a factor of 10 with respect to the KRM, L_X does not diminish by the factor of 100 that one could expect as a rule of thumb (the cooling per unit volume being $\propto \rho^2$): the much lower than expected reduction of L_X is thus due to different hot gas distributions between the two models.

We finally point out that the noisy temporal behavior of L_X is a consequence of the density and temperature fluctuations associated to large eddies in the flow.

3.1.3. *Surface Brightness*

The X-ray surface brightness (Σ_X) evolution of model A1 is shown in Figure 4 at the same epochs of the shots in Figure 1. The optical isophotes (Σ_*) are also superposed for comparison, and the galaxy is seen perfectly edge-on.

During the wind phase, the X-ray isophotes are peanut shaped, with regular lobes aligned with the galactic polar direction (Fig. 4*a*). The elongation of the isophotes decreases steadily with time; they become rounder and rounder; and, in the inner regions, eventually flatter than the optical isophotes (Figs. 4*b* and 4*c*). The isophotes of Σ_X at the present epoch are rather flat in the central regions and become progressively circular moving outward. This is due to the well-known fact that the emitting gas accommodates in a potential well that is more spherical at large r. The irregularities in the isophotal shapes are clear evidence of the inner turbulence (Fig. 4*d*).

Note that once the cold filaments appear (Fig. 4*b* and 4*c*), Σ_X becomes very disturbed: we stress however that such an effect is magnified in our simulations by the imposed geometry, in which the filaments are in fact surfaces. We also computed Σ_X under different viewing angles. It turns out that at early epochs the X-ray isophotes appear still elongated along the optical minor axis, even for values of the viewing angle as low as 45° (90° = edge-on). Instead, at late epochs, Σ_* and Σ_X become very similar as soon as the inclination angle is slightly lower than 90°.

3.1.4. *Model A2:* $\vartheta_{\rm SN} = 0.3$ *and* $k = 0$

We describe here a model very similar to A1, but with $k = 0$, all the galaxy flattening being due to σ_φ^2 (see Table 1). For this model the value of χ is independent of any assump-

[3] The formation of such filaments seems to be a rather general feature in decoupled flows such as this. Melia, Zylstra, & Fryxell (1991), for instance, find astonishingly similar structures in their studies on accretion disk coronae around black holes.

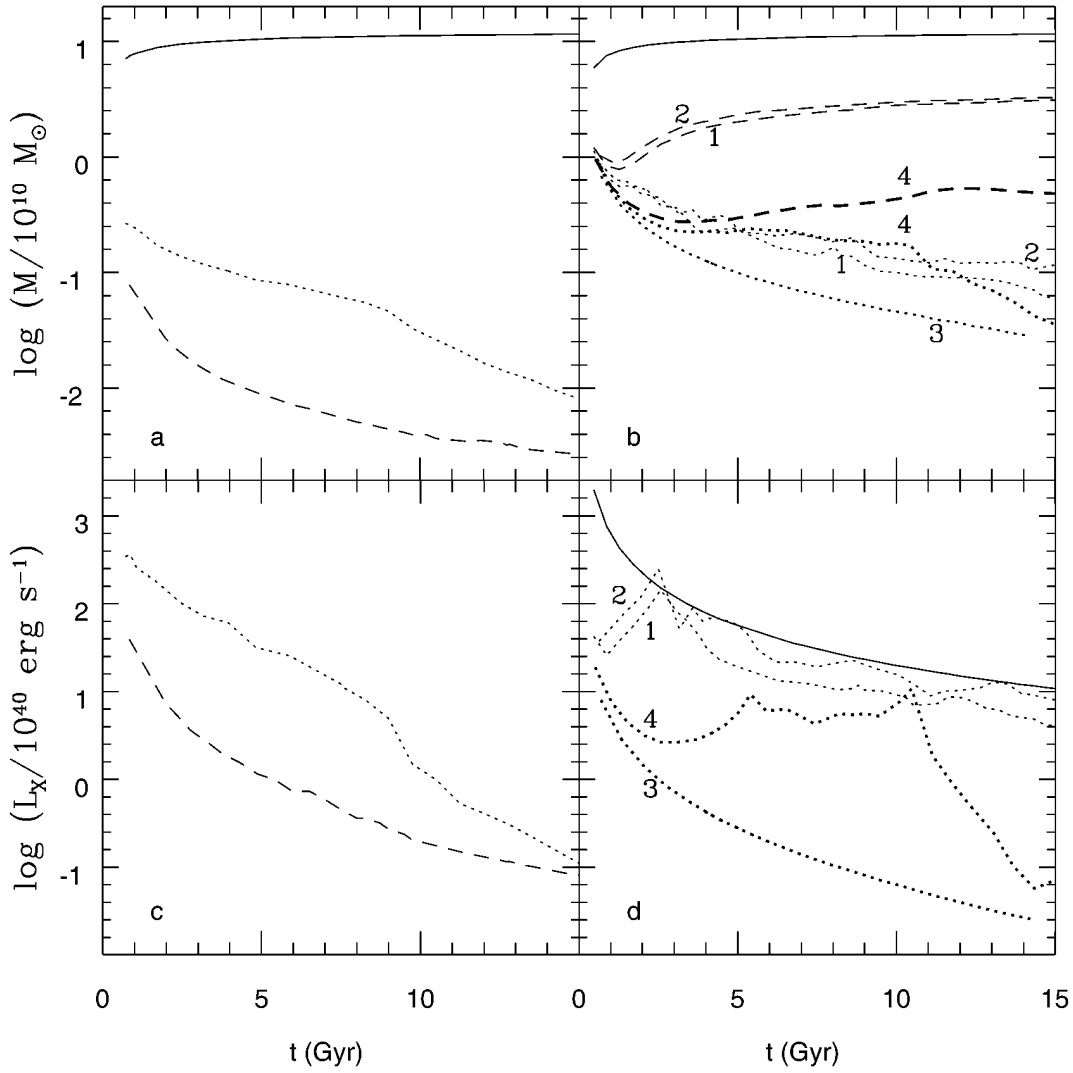

FIG. 3.—Time evolution of the mass and luminosity of gas flows for the models discussed in the text. Panel (*a*) illustrates the behavior of the hot gas of model B1 ($\vartheta_{SN} = 0$, $k = 1$; *dashed line*) and of model B2 ($\vartheta_{SN} = 0$, $k = 0$; *dotted line*). The solid line represents the total mass lost by the stars. Panel (*c*) represents the L_X evolution for the same models. Panel (*b*) shows the mass budget for the models with $\vartheta_{SN} = 0.3$. Dotted lines represent the evolution of the hot gas mass for model A1 ($k = 1$, *line 1*), A2 ($k = 0$, *line 2*), C1 ($k = 1$, *line 3*), and D1 ($k = 1$, *line 4*). Dashed lines show the total gas mass inside the galaxy. The solid line again represents the total mass lost by the stars. Panel (*d*) shows the evolution of L_X for these models (*dotted lines*), and the solid line represents L_{SN}.

tion on the thermalization of ordered motions (see eq. [12] with $\gamma = 0$) and is equal to unity.

From Figure 3*b* it is apparent how this nonrotating model has a higher total gas mass (*dashed line 2*) than the rotating model A1 (*dashed line 1*). This is because rotation—if not entirely thermalized—decreases a $\chi < 1$ (see § 2.3), and in fact the largest difference between dashed line 1 and dashed line 2 takes place during the initial wind phase, when χ is substantially lower than unity. Also the hot gas mass of model A2 (*dotted line 2*) is higher than that of model A1 (*dotted line 1*): this is due to the combined effect of rotation, already discussed, and of the presence of a slightly more massive cold disk in model A1, a consequence of angular momentum conservation. This effect is quite small in the models heated by SNIa but much more important in the cooling-flow models (a more detailed discussion is postponed to § 3.2).

The main features of the temporal evolution of L_X are similar for models A1 and A2 (Fig. 3*d*, *dotted line 2*). We note however that the L_X of model A2 is slightly higher than that of model A1, in accordance with its higher content of hot gas. The flow dynamical evolution of model A2 is also quite similar to that of model A1. The transient phase of filamentary instabilities—although to a minor extent—is still present and develops approximately at the same time as in model A1. The absence of rotation does not affect the presence of oscillations in the temporal evolution of L_X, thus indicating that the turbulence is mainly due to a decoupled inversion of the gas flow, rather than to rotation. Finally, Σ_X evolves mainly as in model A1, although the X-ray isophotes appear more circular in this nonrotating case.

3.1.5. *Models A3 and A4:* $\vartheta_{SN} = 0.3$ *and* $k = 1$ *but Different a/b's*

We focus here on the relationship between the galaxy's flattening and the development of the cold instabilities. To investigate this point, we run two models similar to model A1, except for the ratio a/b (see Table 1). A quantitative measure of the flattening of a MN model in its central regions is obtained with a series expansion of equation (1).

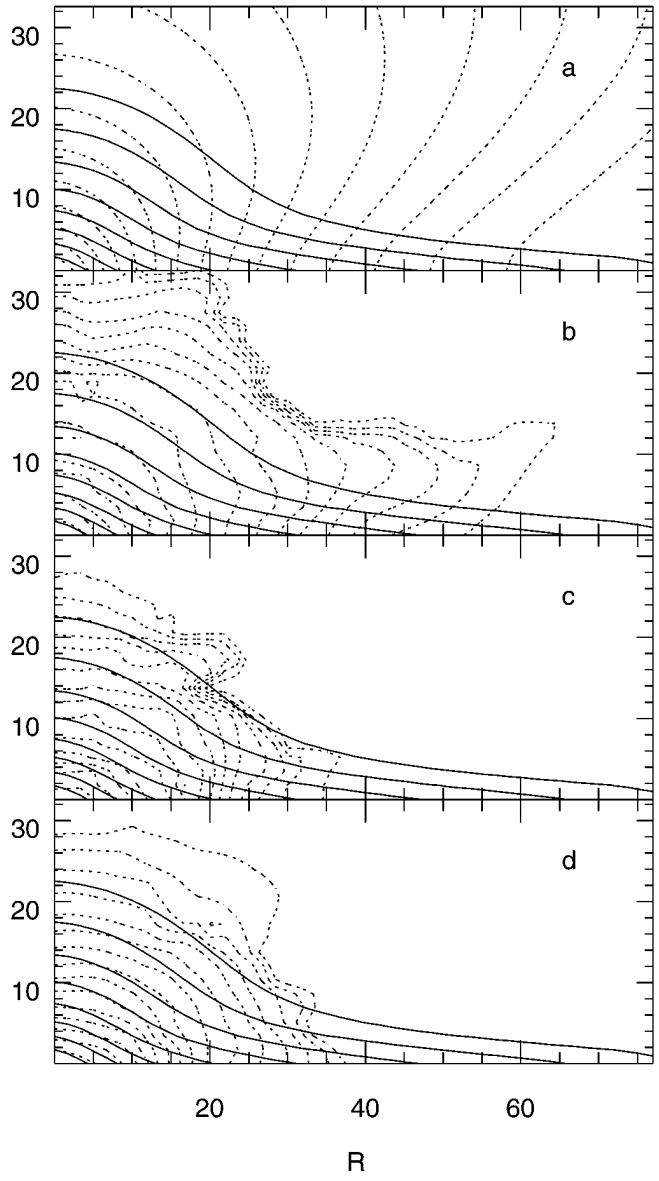

FIG. 4.—Optical (*solid lines*) and X-ray (*dotted lines*) surface brightness distributions for model A1, at the same representative times as in Fig. 1 (time increases from top to bottom). The optical isophotes are separated by 1 order of magnitude. The X-ray isophotes are logarithmically spaced: the lowest value (-8.51 in cgs units) is the same in all panels, the maximum is (*a*) -3.34, (*b*) -2.97, (*c*) -3.37, and (*d*) -4.47.

Retaining the quadratic terms, the resulting isodensity surfaces are similar ellipsoids whose ellipticity is

$$\mathscr{E}_\rho = 1 - \sqrt{\frac{s+5}{(s+1)(s^2+4s+5)}}, \qquad (13)$$

where $s = a/b$. Thus, $s = 1$ adopted in models A1 and A2 corresponds to $\mathscr{E}_\rho = 0.45$. As a consequence, with $s = 0.7$ (and $\mathscr{E}_\rho = 0.36$), model A3 is slightly more spherical than model A1, and its $\chi = 1.2$ is higher, as expected. The result is that the flow inversion occurs earlier, and the filamentary phase is already completely developed at $t_{\rm fil} = 1.4$ Gyr. On the contrary model A4, with $s = 1.3$ and $\mathscr{E}_\rho = 0.52$, is flatter. Its $\chi = 0.94$, and the filamentary phase starts now at $t_{\rm fil} = 3$ Gyr. For a short time this model shows the contemporary presence of two cold structures similar to that in Figure 2. These two models show how small changes in the galaxy flattening can change the flow evolution in the CDPR scenario.

3.2. *Model B1:* $\vartheta_{\rm SN} = 0$ *and* $k = 1$

A very different flow evolution is obtained by suppressing the SNIa heating in a model equal to A1: now $\chi = 4$ since the beginning, and the behavior is that of a pure cooling flow. The velocity field is very smooth, thus showing that SNIa's play a fundamental role in maintaining a boiling hot gaseous halo. In this case we do not obtain the transient filamentary structure, and L_X decreases smoothly. The present-day L_X is more than 1 order of magnitude lower than in the previous SNIa heated cases (Fig. 3*c*, *dashed line*), because there is considerably less hot gas in the galaxy (Fig. 3*a*, *dashed line*). The cooling gas accumulates now on an extended cold disk of $\simeq 10^{11}\ M_\odot$, approximately 10 times more massive than that of model A1. Such a disk, present also in the simulations of BM and KM, is not actually observed in real galaxies. The X-ray isophotes of model B1 closely follow the optical ones.

3.2.1. *Model B2:* $\vartheta_{\rm SN} = 0$ *and* $k = 0$

Model B2 is analogous to model B1, but no ordered rotation is applied. In this case L_X is higher than in model B1 at every time (Fig. 3*c*, *dotted line*), just due to the larger amount of hot gas (Fig. 3*a*, *dotted line*). At first sight it could seem contradictory that the model with the lower L_X (B1) has cooled a larger amount of gas; i.e., one could expect a higher L_X, at least in the past. However, although more mass cools per unit time in the rotating model, the lack of thermalization of the gravitational energy of the gas that stops on the rotating cold disk instead of falling into the galaxy center produces a net quenching in the global L_X (as pointed out by BM). The Σ_X isophotes in the nonrotating case are more concentrated toward the center and rounder than in the rotating case, as found by BM.

It is of interest to compare our cooling flow models with those of BM. These authors find a dramatic reduction of L_X when introducing rotation, but at variance with us, the hot gas mass in their rotating models decreases only slightly compared with the nonrotating ones. Thus, the lower luminosity in their rotating models is due essentially to a redistribution of the hot gas mass, rather than to its scarcity, as in ours. The origin of this different behavior is in the higher flattening of the models used here (i.e., in the presence of the disk in the MN density distribution). In fact, in our models a larger fraction of gas is produced at low z over the galactic equatorial plane. When the model is rotating, this gas falls on the disk approximately at the same distance from the center where it was formed, because of angular momentum conservation. So, on one hand, it releases a much lower gravitational energy, and, on the other, the hot gas distribution is changed only slightly with respect to the nonrotating case. The accumulation of the gas on the disk also significantly increases its cooling, and the final result is a reduction of the hot gas mass. Note that also in the BM models the amount of cold gas increases with an increasing ellipticity of the parent galaxy.

3.3. *Models C1 and D1:* $\vartheta_{\rm SN} = 0.3$ *and* $k = 1$

As mentioned in § 1, we also ran models which are similar in many aspects to A1, but with larger b's, in order to have realistic values for the velocity dispersion (see Table 1). Since $\rho_*(0) = M_*(3+s)/4\pi b^3(1+s)^3$, increasing b at fixed s produces a reduction in the gas density and thus in the

cooling, because of the lower stellar density. At the same time, because $\Phi_*(0) = GM_*/b(1 + s)$, L_g is reduced as well, favoring the escape of the gas.

Model C1 ($b = 4$ kpc, $\sigma_c = 290$ km s^{-1}, $v_{rot} = 309$ km s^{-1}, $\chi = 0.85$) develops a decoupled inflow at 5.5 Gyr, as can be seen from the evolution of L_X (Fig. 3*d*, *heavy dotted line 3*). The most striking feature is again the formation of cold filaments (Fig. 5). Surprisingly enough, these filaments do not form at the moment of flow inversion ($t_{cc} \simeq 5.5$ Gyr), but quite later ($t_{fil} \simeq 10.5$ Gyr). At variance with model A1, they form close to the galactic equatorial plane (cf. Fig. 2). Once on the plane, they slowly drift toward the center and accrete on a small cold disk ($r \sim 4$ kpc, $M_{disk} \simeq 510^9 M_\odot$). This dynamical phase is characterized by a conspicuous and steady decrease of L_X, a consequence of the decrease of the hot gas mass (Fig. 3*b*, *heavy dotted line 3*). While this effect is certainly real, it is magnified in our simulations for two reasons. First, as already pointed out, the filaments are in fact cylindrical surfaces; second, as usual in two-dimensional simulations, reflecting boundary conditions on the disk introduce nonphysical effects favoring cold material accumulation. The Σ_X evolution is similar to that of model A1, but postponed in time.

For model D1 ($b = 5$ kpc, $\sigma_c = 258$ km s^{-1}, $v_{rot} = 277$ km s^{-1}, $\chi = 0.7$), the resulting flow is a pure wind all over the galaxy, lasting for all the Hubble time without any decoupling. All the gas is hot, and its mass—as is common in the wind phase—decreases steadily and is very low (Fig. 3*b*, *heavy line 4*). L_X is also very low and decreases proportionally to the gas mass (Fig. 3*d*, *heavy dotted line 4*). Σ_X is similar to that shown in Figure 4*a*. This run clearly shows how in a realistic flat model, even with a low ϑ_{SN}, the flow can be in the wind phase during its entire evolution.

3.3.1. *Models C2 and D2: $\vartheta_{SN} = 0.3$ and $k = 1$, but different a/b's*

We now briefly describe the behavior of two models similar to C1 and D1, but with different flattening (see Table 1). The first (C2, $s = 1.3$, $\mathscr{E}_\rho = 0.52$, $\chi = 0.75$) is flatter than model C1 and, consequently, has a lower χ. The resulting flow is a wind during all the time. This model (with $b = 4$ kpc) is energetically very similar to D1 ($s = 1$ and $b = 5$ kpc), as testified by their χ values, and its flow evolution is also similar.

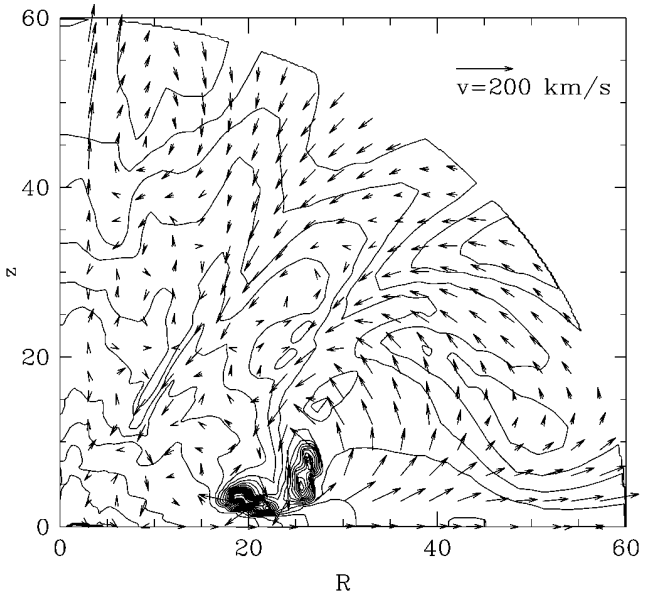

FIG. 5.—Gas temperature and velocity for model C1 at $t \simeq 10$ Gyr, when the cold filament is completely developed.

Model D2 ($b = 5$ kpc, $s = 0.6$, $\mathscr{E}_\rho = 0.33$, $\chi = 0.86$) is obtained from D1 by decreasing its flattening. As a consequence the gas is more bound as testified by a χ similar to that of model C1 ($s = 1$ and $b = 4$ kpc). The resulting evolution is similar to that of model C1, with the flow inversion and the following development of a decoupled inflow around $t_{cc} \simeq 5.5$ Gyr. However, in this case no cold filaments are developed. In conclusion, a very small change in the flattening can compensate for a variation of the characteristic scale length, showing again the strong sensitivity of models to variations of galactic structural parameters in the CDPR scenario.

4. DISCUSSION

Although the number of models we ran is not sufficient for an accurate statistical and quantitative analysis of the gas flow properties in flat and rotating galaxies, a qualitative comparison with the spherical models discussed in CDPR and with cooling flow models is possible; it is also interesting to compare our results with recent observational findings (Pellegrini, Held, & Ciotti 1997).

In order to compare the behavior of S0 models with the equienergetical spherical models discussed in CDPR, we performed calculations for model galaxies with $\chi = 1$ at the present epoch (models A1 and A2). We stress again that while $\chi = 1$ is a quite natural product of realistic spherical models, it turns out to be rather extreme for flat models. In any case, in flat models a clear X-ray underluminosity with respect to their spherical counterpart is found, mainly due to a drastic reduction of the hot gas mass. The amount of galactic rotation contributes only slightly to such a reduction.

We also ran a few models with $\vartheta_{SN} = 0$ (models B1 and B2). These have a remarkably low L_X, in contrast with spherical cooling flows, which in general show excessively high X-ray luminosities. Although the model without rotation displays a present-day L_X similar to that of the rotating model, it was much more luminous in the past. As a consequence, with different choices of the structural and dynamical parameters, a large difference in the L_X can be obtained. Such a possibility is supported also by the models of BM, where different degrees of rotation lead to a spread in L_X.

When the galaxy structure and dynamics are more similar to those of observed galaxies, and SNIa's are present, χ is low, and the galaxy is permanently in a global wind phase or loses a large amount of gas during a Hubble time; the flow decoupling takes place at late times, even for ϑ_{SN} as low as 0.3. The qualitative predictions made in CP are thus correct: it is much easier to extract gas from a flat, realistic galaxy model, than from a rounder system of the same L_B. L_X may span all the values in the range between that of a pure wind and approximately L_{SN} by, for instance, varying b or the galaxy flattening, similarly to what happens for spherical models in the CDPR scenario for small variations of the model parameters.

Moreover, the X-ray underluminosity of flat galaxies can naturally be accounted for because their L_X never reaches L_{SN}, even in the inflow phase. A possible explanation of the observations could be that at low L_B, where the CDPR scenario predicts a significant number of objects to have an energy budget sufficient to unbind the gas, flat galaxies are

preferentially found in the wind phase with respect to spherical galaxies of the same optical luminosity, while at high L_B, where a significant number of galaxies contain inflows, the underluminosity of flat galaxies could be due to the underluminosity of their inflow phase, as found (albeit for different reasons) in our models and by BM.

We computed also a few models (not shown here) with a different flattening of the dark matter distribution with respect to the stellar component. The results are qualitatively similar to those discussed above. As a general rule, for a given stellar distribution, a rounder halo increases χ and reduces $t_{\rm fil}$. For example, a model similar to A1, but with a spherical halo $(a/b)_h = 0$, has $\chi = 1.14$ and $t_{\rm fil} \simeq t_{\rm cc} = 1$ Gyr; a model similar to C2, but with a rounder halo $(a/b)_h = 0.6$, has $\chi = 0.8$ and $t_{\rm fil} \simeq 6.2$ Gyr. As expected, as the flattening of the dark halo increases, χ decreases and $t_{\rm fil}$ increases: for example, a model similar to D2 but with $(a)_h = 1.3$ always remains in the wind phase, in accordance with the lower value of $\chi = 0.79$.

We conclude that, on the basis of L_X alone, it is not possible to decide whether the CDPR scenario or the cooling flow scenario is more suitable to describe the flows in S0s and Es: both can reproduce the X-ray underluminosity of flat galaxies. The *scatter* in the $L_X - L_B$ diagram (at a fixed optical luminosity) is mainly produced by the galactic flattening (and rotation to a minor extent) in the CDPR scenario and by the amount of rotation in the cooling flow models.

In any case, the current explanations of the observational results are unsatisfactory. In fact, Pellegrini et al. (1997) pose unsolved problems, especially concerning the explanation of the scatter in the $L_X - L_B$ diagram, as a function of the flattening and rotation. It is found that L_X/L_B does not correlate with rotation and/or flattening. On the contrary, a very strong *segregation* effect is found: only galaxies with small flattening and low $v_{\rm rot}/\sigma_c$ show a scatter in L_X/L_B, while flat objects and strongly rotating ones are systematically found only at low L_X/L_B. The main factor in determining the L_X/L_B segregation (and scatter, as a consequence) could be related to the *slope* of the galaxy surface brightness profile in the very center, as measured by *Hubble Space Telescope* observations (Pellegrini 1997 and references therein). This would tell us that a *nuclear* origin for the X-ray behavior of early-type galaxies should be taken into proper account (Ciotti & Ostriker 1997). It is remarkable how the *independently chosen* separation of early-type galaxies in cuspy and core galaxies, a separation operated using only photometric criteria, reproduces exactly the segregation in the $L_X - L_B$ plane: while core galaxies show the entire scatter in L_X at fixed L_B, cuspy galaxies are invariably found only at low L_X.

Other problems affect both the CDPR models and the cooling flow models. For example, the absence of massive cold disks in Es seems to support the CDPR scenario, while the claimed very low metallicity in the hot gas is against it, because a low metallicity contrasts with the assumption of a nonnegligible value of $\vartheta_{\rm SN}$. In fact, in principle, constraints on the SNIa rate can be given by estimates of the iron abundance in galactic flows (see, e.g., Renzini et al. 1993 and references therein). Under the assumption of solar abundance ratios, the analysis of the available data suggests a very low iron abundance, consistent with no SNIa's enrichment and even lower than that of the stellar component (Ohashi et al. 1990; Awaki et al. 1991; Ikebe et al. 1992; Serlemitsos et al. 1993; Loewenstein et al. 1994; Awaki et al. 1994; Arimoto et al. 1997; Matsumoto et al. 1997). This is rather puzzling, in that a value as high as $\vartheta_{\rm SN} = 0.3$ agrees with the current optical estimates of the SNIa rates. However, some authors have found that more complex multitemperature models with higher abundance give a better fit to the data (Kim et al. 1996; Buote & Fabian 1997). So, there are arguments on both sides of the abundance question, which is far from being a closed issue. In any case, it is clear that the CDPR scenario is ruled out in case a null SNIa rate is clearly determined.

An interesting feature of our models, which could be used to discriminate between the CDPR and the cooling flow scenario, is the spontaneous occurrence of the flow decoupling. This is at the origin of the striking feature of the transient cold filaments, which—if caught during their formation—should be observed first as soft X-ray–emitting structures and, subsequently, as Hα filaments. In model A1 this takes place at $t_{\rm fil} \simeq 2$ Gyr, while in model C1 (the model with $b = 4$ kpc but similar to A1 in all other input parameters) it occurs at $t_{\rm fil} \simeq 10$ Gyr. Because of this sensibility to the galaxy structure, it is plausible that for a few galaxies the decoupling of the flow takes place at the present epoch, and so these Hα features could be observed.[4] Indeed, it is tempting to identify the transient cold filaments with the soft X-ray clumps (Kim & Fabbiano 1995) or Hα filaments (Trinchieri & di Serego Alighieri 1991; Trinchieri, Noris, & di Serego Alighieri 1997) recently observed. We note how the size of the numerical and observed structures (on the order of ~ 10 kpc) are surprisingly similar. This could be an alternative explanation to the *galactic drips* proposed by Mathews (1997).

A final comment is on the X-ray surface brightness distributions of the computed models. As already found by BM for cooling flow models, rotation is the key factor in determining whether Σ_X is more or less round than Σ_*, even in the presence of SNIa heating: rotation produces a flatter Σ_X. A favorable feature of the CDPR scenario is that outflowing galaxies have rounder X-ray isophotes, which alleviates the problem of excessively flat Σ_X profiles, affecting our cooling flow models, as well as the models of KM and BM. A detailed observational analysis of the relationship between optical and X-ray surface brightness for the E4 galaxy NGC 720 and S0 galaxy NGC 1332 has been carried out by Buote & Canizares (1997 and references therein). While data for NGC 1332 are more uncertain, an analysis of the X-ray isophotes of NGC 720 shows that they are misaligned with and rounder than the optical ones. The authors conclude that the shape of Σ_X is due to the flattening of the dark halo, which is higher than that of the stellar component. In fact, our simulations shows that, if rotation is the origin of flattening of the X-ray isophotes, then a *decreasing* flattening of Σ_X with galactocentric radius is expected, at variance with the observations. On the other hand, in our simulations flatter dark halos produce (during the inflow phase) flatter X-ray isophotes, as expected.

5. CONCLUSIONS

We have performed two-dimensional numerical simulations of gas flows in S0 galaxy models with different flat-

[4] Note that a flow decoupling—due to different physical reasons—is shown also in spherical power-law galaxies with low dark matter content and low SNIa heating (Pellegrini & Ciotti 1997).

tening, following the same recipe for the input physics adopted in CDPR, and exploring the effects of different amounts of ordered rotation and SNIa energy injection rates, and structural parameters. As a general rule, the WOI sequence that occurs in the one-dimensional models is replaced by a wind phase followed by a decoupled inflow. The main results can be summarized as follows:

1. As expected, models without SNIa heating ($\chi = 4$) host a cooling flow from the beginning. The flow is considerably ordered, and essentially all the gas lost by the stars is cooled and accumulated in the galactic center. If rotation is present, the cold material settles in a disk on the galactic equatorial plane.

2. Models with SNIa heating and $\chi \simeq 1$ at the present epoch invert their flow much earlier than the spherical ones with the same energy budget. In particular, as the SNIa rate decreases, the flow tends to revert its motion starting from the galactic polar regions. In this phase of strong decoupling, cold filaments are created at the interface between inflowing and outflowing gas. This strongly unstable phase lasts ~ 2 Gyr, after which the filaments are definitively accreted on the galactic center. Later on, the turbulences are unable to create regions of very cool, dense gas. The temperature may, however, fluctuate, and gas cooler than X-ray temperatures is present. In the rotating model, the presence of SNIa greatly reduces the formation of the cold disk. In general, less cold matter is present in these models ($\simeq 10^{10}$ $M_\odot$) than in those with $\chi = 4$ ($\simeq 10^{11}$ $M_\odot$).

3. Models with realistic values of the dynamical quantities are characterized by low χ-values. While for model D1 ($b = 5$ kpc, $\chi = 0.7$), the flow is always escaping without displaying any interesting feature, in model C1 ($b = 4$ kpc, $\chi = 0.85$), the flow inversion occurs at $t_{cc} = 5.5$ Gyr, and filaments form at $t_{fil} \simeq 10.5$ Gyr. Of course, no cold mass is present in the first model; in the second, 5×10^9 $M_\odot$ of cold gas form a small disk.

4. For any fixed value of ϑ_{SN}, rotating models are X-ray fainter than the nonrotating ones, for the presence of the cold disk as well as for a different distribution of the hot gas. When compared to one-dimensional models, two-dimensional models are much fainter in the X-rays. The former flows, in fact, have L_X similar to or even higher than L_{SN} after the flow inversion; the latter, instead, always have $L_X < L_{SN}$. This is due to several combined factors: the loss of a SNIa energy fraction that is emitted by the gas below the X-ray temperature in high-density regions (which are much larger than in spherical models); the loss of an SNIa energy fraction used by the gas still outflowing from the external regions of the disk; the corresponding gravitational energy not released by this escaping material; and, for rotating models, the loss of thermalization of the gravitational energy of the cold disk. Another main difference of the temporal evolution of L_X is its noisy behavior in two-dimensional models. This is due to the presence of turbulence and to the formation of cold filaments.

5. We have shown that the flattening of the galaxy in the CDPR scenario allows for a decoupling of the flow, in which different flow regimes are present in different part of the galaxy at the same time. We have found also that the flow decoupling is a general feature; i.e., all our models, except those without SNIa heating and the model with χ substantially lower than unity, show a flow decoupling. We note, however, that the L_X associated to a decoupled flow when $\chi < 1$, is not high: it is true, on the contrary, that *the flows are decoupled even when* $\chi > 1$, as the galaxy loses gas from the disk even with a low SNIa rate. So, the energetical analysis carried out by CP is shown to be qualitatively verified: objects with a low χ-value are found preferentially at low L_X, and, at variance with the cooling flow models, the effect of the flattening is shown to be important in determining the flow evolution.

6. For nonrotating, inflow models, the edge-on Σ_X is rounder than the corresponding Σ_* of the parent galaxy; when rotation is present, Σ_X becomes flatter and very similar to Σ_*. For models with SNIa heating, the Σ_X morphology evolves with time, from a smooth, peanut-shaped geometry to a generally rounder shape than the stellar profile, through disturbed phases during the presence of cold filaments. When rotation is present, in the galactic center, the Σ_X isophotes are somewhat flatter than Σ_*, at variance with nonrotating models in which Σ_X remains more spherical up to the center. As a general rule, even for low line-of-sight inclination angles over the galactic equatorial plane, the isophotes of Σ_X and Σ_* tend to become similar.

All these new features considerably enrich the old CDPR scenario and represent a step further in the direction of a more realistic simulation of a situation that is proving to be very complex. In future, we plan to perform numerical simulations of gas flows in models tailored on observed X-ray–emitting S0 galaxies, in order to improve our understanding of the much richer phenomenology of aspherical gas flows.

We would like to thank James Binney, Fabrizio Brighenti, Silvia Pellegrini, and Ginevra Trinchieri for useful discussions and the referee for comments that improved the paper. We are indebted to Giovanna Stirpe, who carefully read the manuscript. We would also like to thank the CINECA Computing Center for having kindly provided the CRAY C90 for our numerical computations. This work was partially supported by the Italian MURST and the Italian Space Agency (ASI) through grant ASI-95-RS-152.

REFERENCES

Arimoto, N., Matsushita, K., Ishimaru, Y., Ohashi, T., & Renzini, A. 1997, ApJ, 477, 128
Awaki, H., Koyama, K., Kunieda, H., Takano, S., Tawara, Y., & Ohashi, T. 1991, ApJ, 366, 88
Awaki, H., et al. 1994, PASJ, 46, L65
Binney, J., & Tremaine, S. 1987, Galactic Dynamics (Princeton: Princeton Univ. Press)
Brighenti, F., & Mathews, W. G. 1996, ApJ, 470, 747 (BM)
Buote, D. A., & Canizares, C. R. 1997, ApJ, 474, 650
Buote, D. A., & Fabian, A. C. 1997, MNRAS, submitted (astro-ph/9707117)
Cappellaro, E., Turatto, M., Tsvetkov, D. Y., Bartunov, O. S., Pollas, C., Evans, R., & Hamuy, M. 1997, A&A, 322, 431
Ciotti, L., D'Ercole, A., Pellegrini, S., & Renzini, A. 1991, ApJ, 376, 380 (CDPR)
Ciotti, L., & Ostriker, J. P. 1997, ApJ, 487, L105
Ciotti, L., & Pellegrini S. 1996, MNRAS, 279, 240 (CP)
Eskridge, P., Fabbiano, G., & Kim, D. W. 1995a, ApJS, 97, 141
———. 1995b, ApJ, 442, 523
Fabbiano G. 1989, ARA&A, 27, 87
Fabbiano, G., Kim D. W., & Trinchieri G. 1992, ApJS, 80, 531
Ikebe, Y., et al. 1992, ApJ, 384, L5
Kim, D. W., & Fabbiano, G. 1995, ApJ, 441, 182
Kim, D. W., Fabbiano, G., Matsumoto, H., Koyama, K., & Trinchieri, G. 1996, ApJ, 468, 175
Kley, W., & Mathews, W. G. 1995, ApJ, 438, 100 (KM)

Loewenstein, M., Mushotzky, R., Tamura, T., Ikebe, Y., Makishima, K., Matsushita, K., Awaki, H., & Serlemitsos, P. J. 1994, ApJ, 436, L75
Mathews, W. G. 1997, AJ, 113, 755
Mathews, W. G., & Bregman, J. N. 1978, ApJ, 224, 308
Matsumoto, H., Koyama, K., Awaki, H., Tsuru, T., Loewenstein, M., & Matsushita, K. 1997, ApJ, 482, 133
Melia, F., Zylstra, G. J., & Fryxell, B. 1991, ApJ, 377, L101
Miyamoto, M., & Nagai, R. 1975, PASJ, 27, 533 (MN)
Ohashi, T., et al. 1990, in Windows on Galaxies, ed. G. Fabbiano, J. A. Gallagher, & A. Renzini (Dordrecht: Kluwer), 243
Pellegrini, S. 1997, Third ESO Workshop Galaxy on Scaling Relations: Origins, Evolution and Applications, ed. L. N. da Costa & A. Rentini (Garching: ESO), 378
Pellegrini, S., & Ciotti, L. 1997, A&A, submitted
Pellegrini, S., Held, E. V., & Ciotti, L. 1997, MNRAS, 288, 1
Plummer, H. C. 1911, MNRAS, 71, 460
Renzini, A., Ciotti, L., D'Ercole, A., & Pellegrini, S. 1993, ApJ, 419, 52
Satoh, C. 1980, PASJ, 32, 41
Serlemitsos, P. J., Loewenstein, M., Mushotzky, R., Marshall, F., & Petre, R. 1993, ApJ, 413, 518
Tammann, G. 1982, in Supernovae: A Survey of Current Research, ed. M. Rees & R. Stoneham (Dordrecht: Reidel), 371
Trinchieri, G., & di Serego Alighieri, S. 1991, AJ, 101, 1647
Trinchieri, G., Noris, L., & di Serego Alighieri, S. 1997, A&A, 326, 565